CrystEngComm

ROYAL SOCIETY OF CHEMISTRY

COMMUNICATION

View Article Online
View Journal | View Issue

Cite this: *CrystEngComm*, 2025, **27**, 8

Received 11th October 2024,
Accepted 10th November 2024

DOI: 10.1039/d4ce01036a

rsc.li/crystengcomm

3,5-Dinitro-1-(3,3,3-trifluoropropyl)-1*H*-pyrazol-4-amine as an insensitive and thermostable energetic melt-castable material†

Dangyue Yin, Boqian Yang, Hongyu Lv, Siwei Song, Yi Wang * and Qinghua Zhang *

A trifluoropropyl functionalized energetic compound, *viz.* 3,5-dinitro-1-(3,3,3-trifluoropropyl)-1*H*-pyrazol-4-amine (TFDNPA), was designed and synthesized, which exhibited potential for TNT replacement as an energetic melt-castable carrier in aluminized explosive formulation due to excellent thermal properties (T_m: 100 °C and T_d: 261 °C), good detonation performance (*D*: 7330 m s^{-1} and *P*: 23.3 GPa), low impact sensitivity (IS: 35 J) and enhanced reaction activity with aluminium powders in melt-cast explosive formulations.

Introduction

Energetic melt-castable materials are a special class of energetic compounds with melting points in a narrow temperature range of 70–120 °C.[1,2] This reversible ability to change from a solid phase to a liquid phase makes them irreplaceable carriers in melt-cast composite explosives.[3–5] Due to the high calorific value (31 MJ kg^{-1}), aluminium (Al) powders are usually added to currently widely used composite explosive formulations to increase the detonation heat and detonation temperature.[6,7] However, for traditional melt-cast composite explosive formulations (such as TNT/RDX/Al, DNAN/HMX/Al, *etc.*), Al powders transform into various condensed phase particles (including molten Al droplets, aluminum oxide particles, *etc.*) during the detonation reaction to show an adverse effect on the propagation of detonation waves. In contrast, aluminium fluoride (AlF_3) would be gaseous under the conditions of the detonation reaction to effectively prevent the agglomeration of condensed phase Al particles.[8–10] For this reason, the introduction of fluorine elements into Al-based composite explosives is very beneficial for improving the detonation performance. Therefore, a promising strategy is to develop fluorine-containing melt-castable energetic compounds.

With increasing attention on the high-efficiency energy release of Al-based composite explosives, there has been significant interest in fluorine-containing energetic melt-castable materials.[11–13] At present, several fluorine-containing melt-castable compounds have been reported and they could be divided into three main categories (Fig. 1). Due to the flexible structural feature and high reliable synthesis, fluorodinitroethanol is a widely used structural segment in

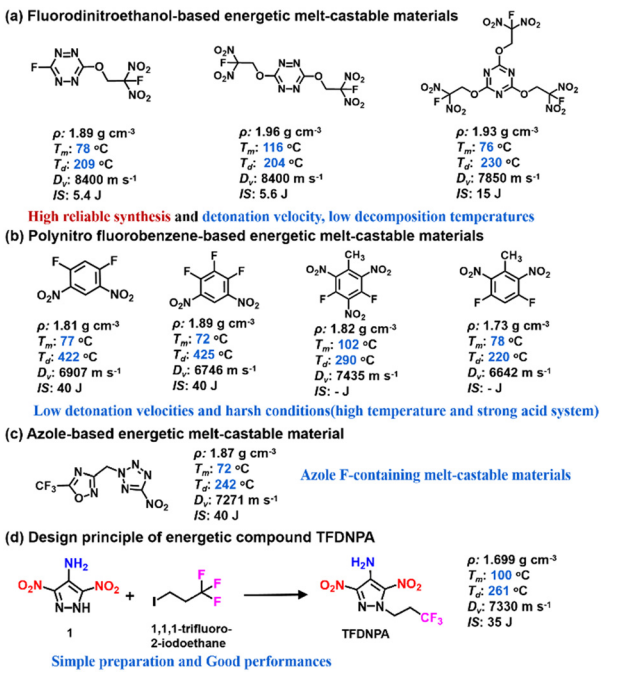

Fig. 1 (a) Chemical structures and properties of fluorodinitroethanol-based energetic melt-castable materials; (b) chemical structures and properties of polynitro fluorobenzene-based energetic melt-castable materials; (c) chemical structure and properties of the azole-based energetic melt-castable material; (d) chemical structures, synthetic route and properties of **TFDNPA**.

School of Astronautics, Northwestern Polytechnical University, Xi'an, Shanxi, 710065, China. E-mail: ywang0521@nwpu.edu.cn, qinghuazhang@nwpu.edu.cn

† Electronic supplementary information (ESI) available. CCDC 2402298. For ESI and crystallographic data in CIF or other electronic format see DOI: **https://doi.org/10.1039/d4ce01036a**

these fluorine-containing energetic melt-castable compounds (Fig. 1a). Although they exhibit high detonation velocities (usually exceeding 8000 m s^{-1}), their decomposition temperatures are relatively low (around 200 °C), which narrows the range of the molten liquid phase and makes them unsuitable for practical applications.[14–17] Polynitro fluorobenzene derivatives are an important type of energetic melt-castable compounds. However, their detonation velocities are usually relatively low (mostly ranging from 6000 to 7500 m s^{-1}) (Fig. 1b). Moreover, introducing nitro groups into the fluorobenzene skeleton usually requires harsh reaction conditions due to the strong electron-withdrawing effect of fluorine atoms.[18,19] For five-membered nitrogen heterocyclic compounds, there are very few options for fluorine-containing melt-castable compounds (as shown in Fig. 1c). Therefore, it is highly desirable to develop new fluorine-containing melt-castable molecules by introducing fluorine into heterocyclic energetic skeletons.[20–23]

In our continuous efforts to develop new melt-castable energetic materials, we have found that the combination of energetic heterocyclic skeletons and flexible substituents is beneficial for regulating the melting point of energetic molecules to meet the requirements of energetic melt-castable materials.[24–27] Here, we have designed a new fluorine-containing pyrazole compound (**TFDNPA**) by integrating 3,5-dinitro-1*H*-pyrazol-4-amine and 1,1,1-trifluoropropane. In addition, **TFDNPA** exhibits excellent properties including high density, good detonation performance, low mechanical sensitivities, *etc.*, (Fig. 1c), demonstrating its good potential as a TNT replacement.

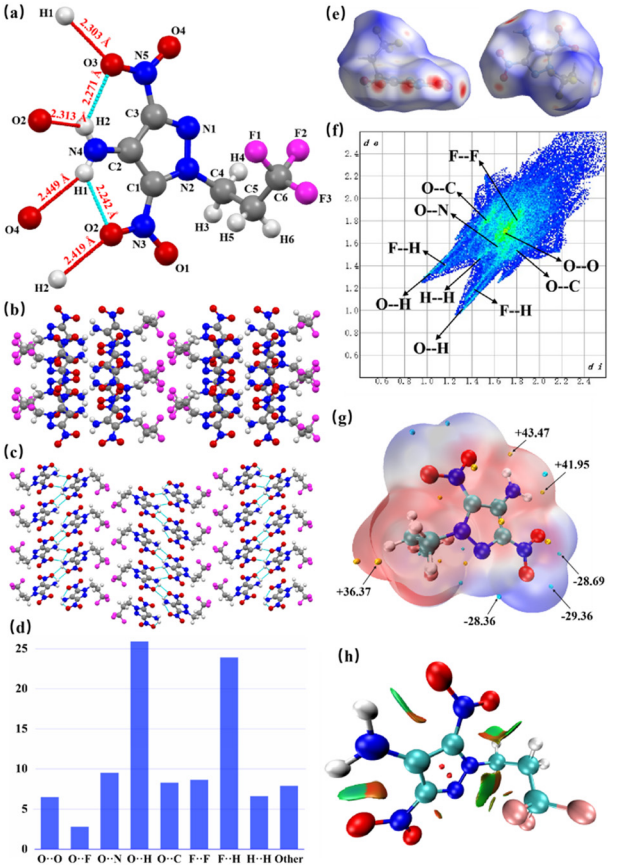

Fig. 2 (a) Crystal structure; (b) crystal stacking diagram along the *a*-axis; (c) crystal stacking diagram with the hydrogen bond network along the *b*-axis; (d) the individual atomic contact percentage contribution to the Hirshfeld surface; (e) Hirshfeld surfaces; (f) 2D fingerprint plot; (g) ESP plot (kJ mol^{-1}); (h) NCI isosurface (isovalue = 0.5).

Results and discussion

Synthesis

As shown in Fig. 1d, the target 3,5-dinitro-1-(3,3,3-trifluoropropyl)-1*H*-pyrazol-4-amine (**TFDNPA**) was prepared by a one-step substitution reaction. First, we synthesized 3,5-dinitro-1*H*-pyrazol-4-amine (**1**) from the reported literature.[28] Then, it was reacted with 1,1,1-trifluoro-2-iodoethane in an alkaline environment to give **TFDNPA** with a yield of 94.3% (see ESI†).

Crystal structure

High-quality crystals of **TFDNPA** (CCDC: 2402298) were obtained by slow solvent evaporation from a saturated ethyl acetate solution (Fig. 2a). **TFDNPA** belongs to the $Pca2_1$ space group, with a crystal density of 1.699 g cm^{-3} at 293 K. Additionally, the five-membered rings of the crystals are nearly coplanar with the nitro and amino groups. The torsion angle of O1–N3–C1–C2, H1–N4–C2–C3 and O3–N5–C3–N1 are −179.98°, 177.91° and 177.09°, respectively. Moreover, each molecule of **TFDNPA** has two hydrogen bond donors that form intramolecular and intermolecular hydrogen bonds with varying distances ranging from 2.242 to 2.449 Å. Through these hydrogen bonds, each individual molecule is connected to form a tight network of hydrogen bonds. Additionally, **TFDNPA** shows a layer-by-layer packing structure (Fig. 2b and c), which can reduce the influence of external stimuli by sliding between layers. Moreover, the trifluoropropyl groups are adjacent to each other, and the amino group is connected to the amino group; these give the **TFDNPA** molecule more hydrogen and halogen bonds, forming a powerful network of intermolecular forces. The 2D fingerprint plot and Hirshfeld surface were handled using Crystal Explorer 21.5,[29,30] as shown in Fig. 2d–f. It is evident that the O···H and F···H hydrogen bonds occupy a large proportion in the intermolecular interactions, which further enhances the thermal and mechanical stability of **TFDNPA** on the other hand. In Fig. 2e, some red areas around the nitro group and the amino group can be seen, which represents the higher electron density in these places due to the strong interactions. The oxygen of the nitro group acts as the hydrogen bond acceptor, and the hydrogen of the amino group acts as the hydrogen bond donor, creating a strong hydrogen bond interaction force here.

To gain more information on the intermolecular forces, electrostatic potential (ESP) analysis was applied to **TFDNPA**.[31,32] In Fig. 2g, the maximum ESP values are +43.71,

+41.95 and +36.37 kJ mol^{-1}, concentrated near the hydrogen atoms, while the electrostatic potential minimum are −29.36, −28.69 and −28.36 kJ mol^{-1}, concentrated near the nitro groups. This is because the oxygen atom obtains more charge when bonding, and the electron shielding on it is strengthened, so that the gravity of its lone pair electrons is weakened and the electron density is reduced, which is the blue region in the figure. While hydrogen loses its charge when bonding, the gravity of its electrons is strengthened and the electron density is increased, which is the red region in the figure. To visualize the intramolecular weak interactions, noncovalent interaction (NCI) analysis was performed. As shown in Fig. 2h, there are numerous green and brown areas around trifluoropropyl groups due to the strong halogen bonding interaction. In addition, there are small green and brown areas between the amino group and the nitro group, suggesting the hydrogen bonding force.[33,34] These analytical results contribute to the evidence of abundant intermolecular forces in the crystals.

Thermal properties

For energetic melt-castable materials, the melting point and thermal decomposition temperature are two important indicators. Therefore, the thermal properties of **TFDNPA** were measured at different heating rates in a nitrogen atmosphere by differential scanning calorimetry (DSC). As shown in Fig. 3a, the melting point of **TFDNPA** is 100 °C at a heating rate of 5 K min^{-1}; this temperature falls within the melting point range of energetic melt-castable materials.[35,36] The thermal decomposition temperature of **TFDNPA** is 261 °C at a heating rate of 5 K min^{-1}. The thermal decomposition temperature is higher than that of its precursor compound **1** (T_d: 178 °C), and comparable to TNT (T_d: 295 °C), showing its excellent thermal stability. In order to analyze the non-isothermal thermal decomposition kinetics of **TFDNPA**, the Kissinger and Ozawa methods were applied, as shown Fig. 3b. The apparent activation energy (E_a) of **TFDNPA** determined by the Kissinger and Ozawa methods is 87.40 ± 0.98 and 92.03 ± 0.98 kJ mol^{-1}, respectively. Both values are close to but slightly lower than that of TNT (E_a: 110.93 kJ mol^{-1}), indicating a slightly lower thermal stability compared to TNT.

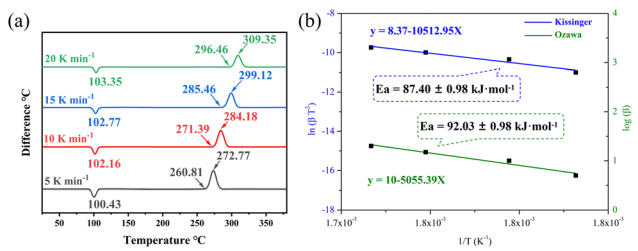

Fig. 3 (a) DSC curves of **TFDNPA** at different heating rates; (b) calculation of the apparent activation energies of **TFDNPA** by the Kissinger and Ozawa methods.

Table 1 Physicochemical properties of **TFDNPA**

Properties	**TFDNPA**	TNT
ρ^a/g cm^{-3}	1.699	1.65
T_m^b/°C	100	80
T_d^c/°C	261	295
Ω^d/%	−65.39	−74.0
ΔH_f^e/kJ mol^{-1}	−563.5	−59.4
D^f/m s^{-1}	7330	6881
P^g/GPa	23.31	19.5
IS^h/J	35	15
FS^i/N	120	360

[a] Density measured at room temperature. [b] Melting point. [c] Decomposition temperature (onset). [d] Oxygen balance. [e] Calculated heat of formation. [f] Detonation velocity. [g] Detonation pressure. [h] Impact sensitivity. [i] Friction sensitivity.

Physicochemical properties

The detonation properties and mechanical sensitivity are also important indicators to reflect the properties of energetic materials. The Gaussian 09 program and atomization method were used to calculate the heat of formation (ΔH_f) of **TFDNPA** as −563.5 kJ mol^{-1} (more details can be found in the ESI†). The large negative heat of formation of ΔH_f is attributed to the introduction of trifluoromethyl (ΔH_f: −447 kJ mol^{-1}) groups. By using the single crystal density and heat of formation, their detonation properties, including detonation velocities and pressures, could be evaluated by the EXPLO5 (version 6.05) program. The detonation velocity and detonation pressure of **TFDNPA** are 7330 m s^{-1} and 23.3 GPa, respectively, which are obviously higher than those of TNT (D: 6881 m s^{-1}, P: 19.5 GPa). In addition, although the friction sensitivity of **TFDNPA** is lower than that of TNT, its impact sensitivity is better than that of TNT. In general, **TFDNPA** exhibits similar properties to TNT (Table 1).

Molecular dynamics simulation

It has been reported that the introduction of fluorine is beneficial to the oxidation of aluminum particles, thereby enhancing the reactivity and energy level of aluminium-containing explosives.[37–39] To explore the effect on compound **TFDNPA**, *ab initio* molecular dynamics (AIMD), which offers high precision, strong universality, and the ability to describe chemical reactions, was applied to analyze the microscopic reaction between Al with **TFDNPA** and TNT, respectively. Details of calculation methods can be found in the ESI.†

The initial layer models of the compound and aluminum after structural relaxation are shown in Fig. S1.† After a 5 ps simulation at 4000 K, a snapshot of the final frame can be seen in Fig. 4a. It is evident that aluminum oxide agglomeration is more obvious in the TNT_AL system compared to that in the **TFDNPA**_Al system. This is caused by the production of aluminum fluoride inhibiting the production of aluminum oxide (Fig. 4a). This result can be validated by observing the smaller coordination number

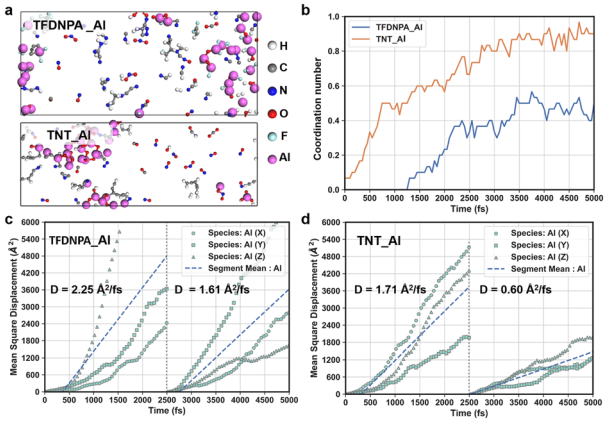

Fig. 4 (a) Screenshot of the last frame of AIMD simulation for TNT_Al and **TFDNPA**_Al systems; (b) the variation of the Al–O coordination number of TNT_Al and **TFDNPA**_Al systems with the number of simulated steps; (c) root mean square displacement of Al atoms in the TNT_Al system; (d) root mean square displacement of Al atoms in the **TFDNPA**_Al system (*D* stands for diffusion coefficient).

between Al and O atoms in the **TFDNPA**_Al system compared to that in the TNT_Al system (Fig. 4b). Besides, during the period from 0 to 2500 ps, the diffusion coefficient (*D*) of the Al atom in the **TFDNPA**_Al system (2.25 $Å^2$ fs^{-1}) is higher than that of the TNT_Al system (1.71 $Å^2$ fs^{-1}). After 2500 ps, even though it decreases to 1.61 $Å^2$ fs^{-1} in the **TFDNPA**_Al system, it is still more than twice as high as that in the TNT_Al system (0.60 $Å^2$ fs^{-1}). These results further indicate that **TFDNPA** can significantly enhance the reaction activity with aluminium by increasing the migration rate of aluminium-containing species and inhibiting the formation and aggregation of aluminum oxide, demonstrating that **TFDNPA** has good application potential in the aluminized explosive formulations.

Conclusions

In summary, a trifluoropropyl functionalized energetic compound **TFDNPA** was efficiently synthesized through a one-step reaction. It exhibits a suitable melting point (T_m: 100 °C), high thermal decomposition temperature (T_d: 261 °C), good detonation performance (*D*: 7330 m s^{-1}, *P*: 23.3 GPa) and low mechanical sensitivity (IS: 35 J). Moreover, AIMD studies suggest that the introduction of fluorine atoms in **TFDNPA** is beneficial for the migration of aluminium-containing species and the inhibition of formation and aggregation of aluminum oxide. This result highlights the potential of **TFDNPA** as an energetic melt-castable material, particularly for aluminized explosive formulations.

Data availability

The data supporting this article have been included as part of the ESI.† Crystallographic data for **TFDNPA** have been deposited at the Cambridge Crystallographic Data Centre (CCDC number: 2402298).

Author contributions

Q. Z. and Y. W. designed and supervised the study. D. Y., H. L. and B. Y. performed the reactions, measurements and data analysis. S. S. performed the crystallographic structural analysis and molecular dynamics simulation. D. Y., B. Y., Y. W. and Q. Z. prepared the manuscript.

Conflicts of interest

There are no conflicts to declare.

Acknowledgements

This work was supported by the National Natural Science Foundation of China (no. 22075259 and 22175157), the Northwestern Polytechnical University Aerospace Power Future Industry Concept Proof Project (24GNYZ0001-06) and the Fundamental Research Funds for the Central Universities (D5000240045 and D5000240065). The authors acknowledge the support from the Beijing Institute of Technology for the EXPLO5 (v6.05) software, and are grateful to Prof. Ping Yin for his kind support in the energetic property calculations.

Notes and references

1 F. Chen, Y. Wang, S. Song, K. Wang and Q. Zhang, *ChemPlusChem*, 2023, **88**, e202300397.
2 L. M. Barton, J. T. Edwards, E. C. Johnson, E. J. Bukowski, R. C. Sausa, E. F. C. Byrd, J. J. Sabatini and P. S. Baran, *J. Am. Chem. Soc.*, 2019, **141**, 12531–12535.
3 F. Hu, L. Wang, Y. Liu, M. M. Hessien, I. H. E. Azab, S. Jing, A. Y. Elnaggar, S. M. El-Bahy, M. Huang and R. Zhang, *Adv. Compos. Hybrid Mater.*, 2022, **5**, 1307–1318.
4 R. Yang, Z. Dong, Y. Liu, Y. Liu, H. Li, G. Zhang and Z. Ye, *Chem. Eng. J.*, 2022, **429**, 132503.
5 N. Sikder, A. K. Sikder, N. R. Bulakh and B. R. Gandhe, *J. Hazard. Mater.*, 2004, **113**, 35–43.
6 Z. Wan, A. T. M. Cruz, Y. Li, Y. Li, Y. Ye, S. Zhu and L. Zhang, *Chem. Eng. J.*, 2019, **360**, 778–787.
7 D. Zhang, J. Shi, B. Wu, R. Zhu, J. Zhou, Y. Guo, C. An and J. Wang, *Mater. Des.*, 2023, **229**, 111874.
8 C. Tu, X. Chen, Y. Li, B. Zhang and C. Zhou, *Def. Technol.*, 2023, **26**, 111–122.
9 S. K. Valluri, M. Schoenitz and E. Dreizin, *Def. Technol.*, 2019, **15**, 1–22.
10 Y. Guo, K. Tan, H. Liu and C. Hu, *Energ. Mater. Front.*, 2023, **4**, 103–109.
11 S. Li and J. Xiao, *Molecules*, 2021, **26**, 4876.
12 N. V. Muravyev, K. Y. Suponitsky, I. V. Fedyanin, I. V. Fomenkov, A. N. Pivkina and I. L. Dalinger, *Chem. Eng. J.*, 2022, **49**, 137816.
13 Q. Liu, H. Wang, Y. Kang, Y. Liu, P. Yu, M. Yuan and H. Gao, *Energ. Mater. Front.*, 2023, **4**, 30–36.
14 Z. Guo, Q. Yu, Y. Chen, J. Liu, T. Li, Y. Peng and W. Yi, *Chem. Rec.*, 2023, e202300108.
15 X. Zhang, M. Fu, F. Zou, J. Hao, Y. Qu, W. Hu and Q. Zhou, *New J. Chem.*, 2019, **43**, 9623–9627.

16 H. Huo, J. Zhang, J. Dong, L. Zhai, T. Guo, Z. Wang, F. Bi and B. Wang, *RSC Adv.*, 2020, **10**, 11816–11822.
17 Z. Li, X. Zhao, F. Gong, C. Lin, Y. Liu, Z. Yang, Q. Yan and F. Nie, *Appl. Surf. Sci.*, 2022, **572**, 151448.
18 C. Huang, Z. Yang, Y. Li, B. Zheng, Q. Yan, L. Guan, G. Luo, S. Li and F. Nie, *Chem. Eng. J.*, 2019, **383**, 123110.
19 J. Ma, C. Bia, X. Yang, X. Guo, B. Li and L. Lu, *J. Mol. Struct.*, 2022, **1264**, 133337.
20 Z. Yan, T. Lu, Y. Liu, W. Liu, B. Zhao, Y. Wang and Z. Ge, *ACS Omega*, 2021, **6**, 18591–18597.
21 Y. Guo, C. Hu, H. Liu and K. Tan, *Energ. Mater. Front.*, 2022, **3**, 177–186.
22 H. Huo, J. Zhang, J. Dong, L. Zhai, T. Guo, Z. Wang, F. Bi and B. Wang, *RSC Adv.*, 2020, **10**, 11816–11822.
23 W. Qian, *CrystEngComm*, 2021, **23**, 3006–3014.
24 A. K. Yadav, M. Jujam, V. D. Ghule and S. Dharavath, *Chem. Commun.*, 2023, **59**, 4324–4327.
25 B. Kuang, T. Wang, C. Li, M. Sun, Q. Tariq, C. Zhang, Z. Xie, Z. Lu and J. Zhang, *Def. Technol.*, 2024, **35**, 100–107.
26 F. Chen, Y. Wang, S. Song, K. Wang and Q. Zhang, *J. Phys. Chem. C*, 2023, **127**, 8887–8893.
27 F. Chen, Y. Wang, S. Song, L. Tan, M. Wei, C. Huang, J. Chen, S. Chen, M. Huang and Q. Zhang, *ACS Appl. Mater. Interfaces*, 2023, **15**, 24408–24415.
28 Y. Zhang, Y. Huang, D. A. Parrish and J. M. Shreeve, *J. Mater. Chem.*, 2011, **21**, 6891.
29 P. R. Spackman, M. J. Turner, J. J. McKinnon, S. K. Wolff, D. J. Grimwood, D. Jayatilaka and M. A. Spackman, *J. Appl. Crystallogr.*, 2021, **54**(3), 1006–1011.
30 M. A. Spackman and D. Jayatilaka, *CrystEngComm*, 2009, **11**, 19–32.
31 T. Lu and F. Chen, *J. Comput. Chem.*, 2011, **33**, 580–592.
32 W. Humphrey, A. Dalke and K. Schulten, *J. Mol. Graphics*, 1996, **14**, 33–38.
33 B. Yang, B. Li, Y. Liu, C. Xu, S. Feng and S. Zhang, *Chem. – Asian J.*, 2024, e202301130.
34 F. Chen, Y. Wang and Q. Zhang, *New J. Chem.*, 2022, **46**, 20540–20553.
35 S. Feng, B. Yang, W. Zhang, B. Li, G. Liu and R. Gou, *J. Mol. Struct.*, 2024, **1296**, 136821.
36 Y. Liu, X. Zhang, J. Li, A. Kou, H. Ding, S. Pang and C. He, *Org. Lett.*, 2024, **26**, 5488–5492.
37 A. K. Yadav, M. Jujam, V. D. Ghule and S. Dharavath, *Chem. Commun.*, 2023, **59**, 4324–4327.
38 J. Wang, W. Cao, R. Liu, R. Xu and X. Chen, *Combust. Flame*, 2021, **229**, 111393.
39 Y. Guo, K. Tan, H. Liu and C. Hu, *Energ. Mater. Front.*, 2023, **4**, 103–109.

